Sensors & Transducers, Vol. 174, Issue 7, July 2014, pp. 53-59

Sensors & Transducers

Research on Power Output Characteristics of Magnetic Core in Energy Harvesting Devices

[1] Rong-Ping GUO, [1] Yong-Xing CAO, [1] Qian PENG, [2] Tian-Chen YUE, [2] Tya-Dong LIU, [2] Ge-Hao SHENG, [2] Xiu-Chen JIANG

[1] Electric Power Research Institute, Sichuan Electric Power Company, Chengdu, 610072, China
[2] Department of Electrical Engineering, Shanghai Jiaotong University, Shanghai, 200240, China
[1] Tel.: 18817519308
E-mail: shenwen1@126.com

Received: 15 February 2014 /Accepted: 30 June 2014 /Published: 31 July 2014

Abstract: Magnetic core is the dominant factor in the performance of current transformer energy harvesting devices. The power output model of the magnetic core is established and verified through experiments. According to the actual application requirements, the concept of power density is proposed. The relationships of power density to air gap, material and dimension of the magnetic core are analyzed and verified through experiments. *Copyright © 2014 IFSA Publishing, S. L.*

Keywords: Inductive energy harvesting, Magnetic core for energy harvesting, Power density, Output characteristics, Energy supply.

1. Introduction

Energy supply is one of the two key technologies for on-line monitoring in transmission lines. Inductive energy harvesting technology, which provides energy support for the monitoring device of the high voltage side, is the main approach for energy harvesting of transmission lines on the high voltage side. The performance of energy harvesting has direct effect on the stability and reliability of on-line monitoring in transmission lines.

Scholars of the world have carried out some preliminary studies on inductive energy harvesting technology in recent years. Most researches focus on circuit design and verification of energy harvesting coils. However, the studies on power output characteristics of energy harvesting and energy harvesting magnetic cores are rare. Literature [1] revealed that maximum power was obtained when the load resistance was equal to the internal resistance of the electricity and energy harvesting coils, and verified the conclusion with a Φ8.5×25×30 mm magnetic core. Literature [2] carried out qualitative analysis of the relationships of the output power of inductive energy harvesting coil to factors such as magnetic conductivity and dimension, but no exact quantitative relationship was given. To prevent the energy harvesting coils from entering the saturation condition when working, literature [3-5] put forward the air gap approach to change the magnetization curve of magnetic cores. In this way, the saturation problem of magnetic cores was solved. In literature [6-9], dual-coil configuration was adopted. When there was overcurrent on the primary side, the compensation coil would be triggered, which improved the dynamic adaptation range of energy harvesting power supply. In literature [10], the secondary current was maintained within the preset range by CT ratio switchover. Literature [11-12] set up the power output model of inductive energy

harvesting magnetic core, and studied the effect on coil output power through the factors such as primary current and secondary coil turns.

In consideration of line safety and signal quality, there are strict limits on the weight of on-line monitoring devices. For example, the weight of the monitoring device on the normal transmission line should not exceed 2.5 kg; the weight of monitoring device on aeolian vibration line should not exceed 1 kg. Therefore, it is necessary to study the power output characteristics of energy harvesting coils and optimize the design of energy harvesting coils, so as to improve its power density 1.

On the basis of the fundamentals principles of current transformer (CT) the power output characteristics of energy harvesting coils under power frequency condition are investigated in the study. The power output model of energy harvesting coils is established. The effects of factors such as air gap, and the material and dimension of magnetic core on the output power of energy harvesting coils are demonstrated.

2. Power Output Model of Energy Harvesting Magnetic Core

The basic working principle of CT energy harvesting device is shown as Fig. 1.

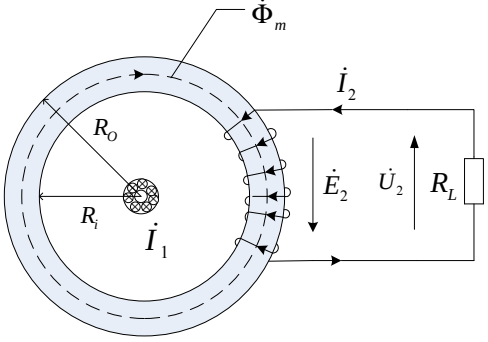

Fig. 1. Principle diagram of energy harvesting device.

According to the basic theory of electric machinery [13], the line on the primary side passes though the magnetic core, and the current is $\dot{I}_1$. The induced electromotive force on the secondary side is

$$\dot{E}_2 = -j\sqrt{2}\pi f N_2 \dot{\Phi}_m , \quad (1)$$

where f is the 50 Hz power frequency, and N_2 is the turns of secondary coil; $\dot{\Phi}_m$ is the maximum value of main magnetic flux. The voltage on resistive load R_L is $\dot{U}_2$, and the internal resistance of secondary coil is R_2. Magnetomotive force balance equation is expressed as

$$y = a * x + b , \quad (1)$$

$$N_1\dot{I}_1 + N_2\dot{I}_2 = N_1\dot{I}_m , \quad (2)$$

where N_1 is 1 turn, $\dot{I}_2$ is the secondary output current and $\dot{I}_m$ is the excitation current. $\dot{I}_m$ can be decomposed into magnetization current component $\dot{I}_\mu$ and core loss $\dot{I}_{Fe}$. Phasor diagram is shown as the left side in Fig. 2. To simplify the analysis, the internal resistance of secondary side and core loss are ignored. Simplified phasor diagram is shown as the right side in Fig. 2.

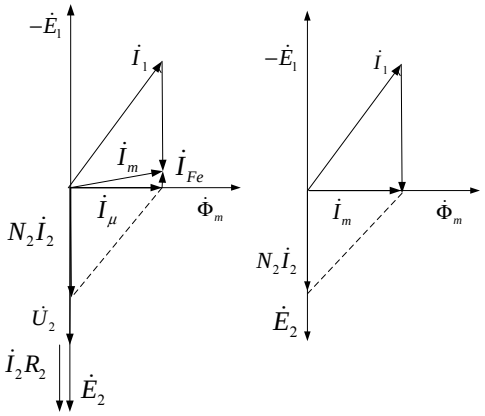

Fig. 2. Phasor diagram and simplified phasor diagram.

At this moment, the magnetization current is the excitation current, which is

$$I_\mu = I_m , \quad (3)$$

The relationship to magnetization current to primary current and secondary current is expressed as

$$I_\mu = \sqrt{I_1^2 - (N_2 I_2)^2} , \quad (4)$$

$$E_2 = \sqrt{2}\pi f N_2 \Phi_m , \quad (5)$$

The maximum value of main magnetic flux is $\Phi_m = B_m S$, where S is the effective sectional area of magnetic core. Suppose that the magnetic core is working in linear region, then the relationship between B_m and H_m is expressed as

$$B_m = \mu H_m , \quad (6)$$

According to Ampere's circuital law

$$H_m l = \sqrt{2} N_1 I_\mu , \quad (7)$$

where N_1 is the turns of the primary side, with the value of 1 here.

The secondary output power is given by

$$P_2 = E_2 I_2 = 2\pi f \mu I_\mu S \frac{\sqrt{I_1^2 - I_\mu^2}}{l}, \quad (8)$$

The magnetization current I_μ is taken as an independent variable. The derivation is taken of formula (8), and assume $P_2'(I_\mu) = 0$. This will result in the maximum output power when $I_\mu = \frac{\sqrt{2}}{2} I_1$ is solved, that is

$$P_{\max} = \pi f \mu S I_1^2 / l, \quad (9)$$

The conclusions from formula (8) and (9) are verified, and an experimental circuit is established as Fig. 3.

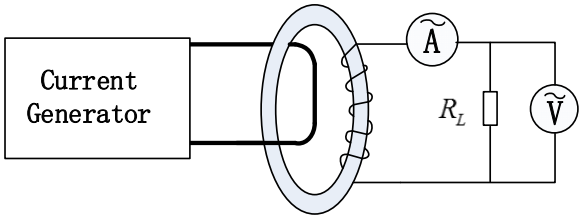

Fig. 3. Diagram of experimental circuit of output power.

The strong current generator provides the primary current. The variable resistive load is connected to the secondary side. The experimental magnetic core is an annular microcrystal alloy magnetic core after bisection using linear cutting. The inner diameter is 55 mm, the external diameter 85 mm, the width 20 mm, 200 turns, average length of magnetic path 213.1 mm, and effective sectional area is 230.3 mm^2. Strong current generator outputs the currents of 10 A, 20 A and 30 A, variable load, and measure the load current and voltage. From formula (4), the excitation current can be obtained. The value is equal to the magnetization current. The relationship between the measured output power and magnetization current is shown as Fig. 4 and 5. It can be seen that the measured curve is in the same dimension as the curve calculated with Matlab. The maximum power value is a little smaller than the theoretical value, and the error is within 10 %. The variation trend of the measured curve slightly lags behind the one calculated theoretically. The reason for the lagging is that the excitation current is approximate to the magnetization current in formula (4). However, due to the existence of core loss component, the magnetization current is smaller than the excitation current. Because the magnetic core can always output its maximum power by controlling the load current [14], the overall shift of the curve towards the right due to the core loss will not affect the effectiveness of this model used for calculating the power output of the magnetic core.

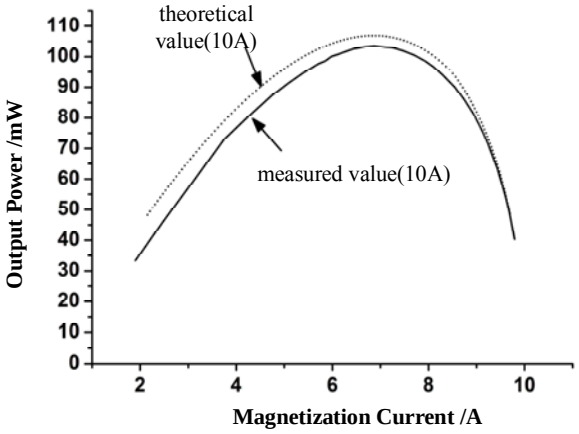

Fig. 4. Measured value and theoretical value (I1=10 A).

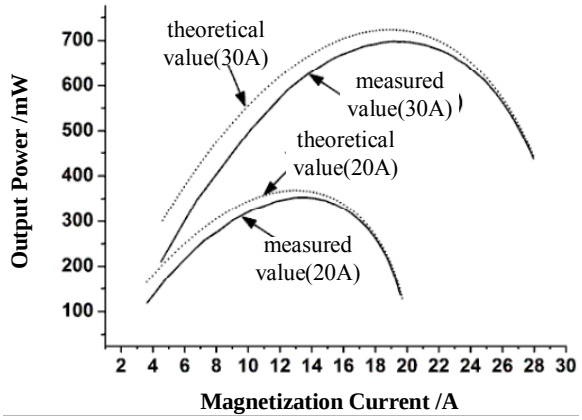

Fig. 5. Measured value and theoretical value (I1=20 A, I1=30 A).

3. Power Density of Energy Harvesting Magnetic Core

To compare the power output capability of the magnetic core, under a certain primary current, the power density λ of energy harvesting magnetic core is defined as the ratio of maximum power output $P_{\max}$ to the magnetic core dimension V .

$$\lambda = \frac{P_{\max}}{V} = \frac{\pi f \mu S I_1^2 / l}{V} \quad (10)$$

3.1. Power Density and Air Gap

Compared with the low reluctance of the soft magnetic material, the air gap has extremely high reluctance. After introducing the air gap, the effective magnetic permeability of the entire magnetic core decreases significantly. Fig. 6 shows the magnetic

core with air gap. The external diameter of the magnetic core is denoted as D_o, the internal diameter D_i, the average length of magnetic path l_c, air gap length as l_g, the relative magnetic permeability before cutting μ_r, absolute magnetic permeability μ, and relative magnetic permeability after cutting μ_{rg}.

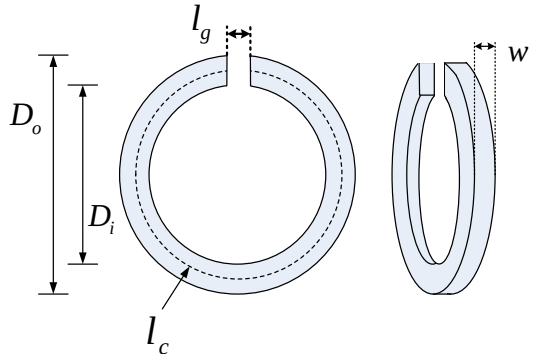

Fig. 6. Magnetic core with air gap.

According to the most common simplified model [15] of magnetic core with air gap, the effective relative magnetic permeability of the magnetic core (including air gap) with air gap is expressed as

$$\mu_{rg} = \frac{\mu_r}{1+\frac{l_g}{l_c+l_g}\mu_r}, \tag{11}$$

The maximum output power of magnetic core with air gap under certain primary current is expressed as

$$P'_{\max} = \pi f \mu_{rg}\mu_0 S I_1^2 / l_c = \pi f \frac{\mu}{1+\frac{l_g}{l_c+l_g}\mu_r} S I_1^2 / l_c, \tag{12}$$

From formula (12), it can be seen that the maximum output power of magnetic core under a certain primary current is very sensitive to the length of air gap. The annular silicon steel magnetic core has an internal diameter of 50 mm, external diameter of 70 mm, width of 35 mm, average length of magnetic path of 183 mm, effective sectional area of 345.4 mm^2 and turns of 200. The experimental circuit is shown in Fig. 3, with variable load resistance. The output curve of magnetic core before cutting under 10 A primary current is measured. It can be seen there is no distortion in the voltage waveform of the magnetic core at the maximum power output. The maximum output power is 869 mW, and the corresponding relative magnetic permeability of 23363 is obtained. Then the magnetic core is subject to bisection with linear cutting technology. Then packing papers of different thickness are added to the joint, as shown in Fig. 7. The power output curve of magnetic core with packing paper under 10 A primary current is measured and compared with the curve before cutting. The result is shown in Fig. 8. The theoretical magnetic permeability and maximum output power of the magnetic core with packing papers of different thickness are calculated from formula (11) and (12). Then the theoretical values are compared with the measured maximum output power. The error is calculated, and the result is as shown in Table 1.

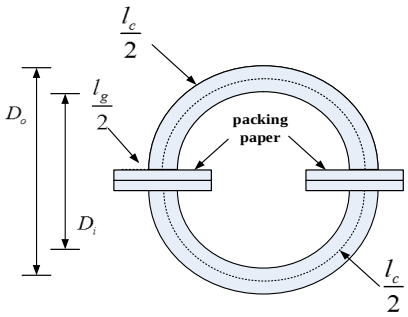

Fig. 7. Magnetic core with packing paper.

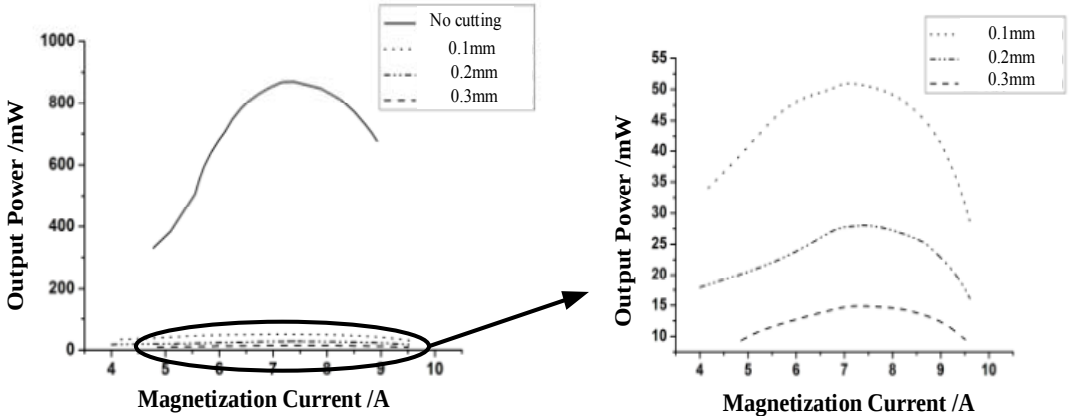

Fig. 8. Output power curves of magnetic core with packing paper.

It can be seen that the error is larger when the thickness of packing paper is used as the length of air gap to calculate the maximum output power. The cutting reversing will cause concave-convex stripes to the section during on-line cutting of magnetic core. Usually, the surface roughness R_Z of the section is 1 μm - 50 μm. Therefore, the air gap introduced by the surface roughness of section after linear cutting is taken into account. The packing paper is removed. The maximum output power of silicon steel magnetic core measured after cutting under 10 A primary current is 258 mW. It can be known from formula (12) that the equivalent air gap length l_{eq} caused by section roughness is about 0.02 mm. The equivalent air gap length (thickness of packing paper plus the section roughness) l_{eq} is taken as the modified equivalent air gap length l_g'. l_g' is used to calculate the theoretical maximum output power under 10 A primary current. The value is compared with the measured value, and the result is shown in Table 2. It can be seen that, when the equivalent air gap caused by linear cutting is taken into account, the maximum theoretical power is almost the same as the measured one in the experiment with packing paper. The error is within 7 %. For the convenience of installation and disassembly, the magnetic core of the energy harvesting device must be subject to bisection before used on the lines. Since no cutting technology and polishing process can guarantee the absolute smoothness of the section, it is inevitable that there will be air gap introduced and the effective magnetic permeability and power density of magnetic core will be bound to decrease after cutting. The surface roughness R_Z by laser cutting can be controlled within 1.6 μm - 6.4 μm, but it costs too much and the cutting thickness should not exceed 20 mm, which is not suitable for cutting the magnetic core for energy harvesting. Under overall consideration, linear cutting is preferred to cut the magnetic core. To decrease the equivalent air gap length caused by linear cutting, the processes such as mechanical polishing should be used to decrease the section roughness.

Table 1. Maximum theoretical value and measured value of maximum output power.

l_g	**Theoretical relative magnetic permeability**	**Maximum theoretical power /mW**	**Measured maximum power /mW**	**Error /%**
0.1 mm	1700.5	63.3	50.6	25.1
0.2 mm	882.8	32.8	28.1	16.7
0.4 mm	450.4	16.8	15.0	12.0

Table 2. Theoretical value and measured value of maximum output power with modified air gap length.

l_g'	**Theoretical magnetic permeability**	**Maximum theoretical power /mW**	**Measured maximum power /mW**	**Error /%**
0.12 mm	1434.6	53.4	50.6	5.5
0.22 mm	805.4	30.0	28.1	6.8
0.42 mm	429.4	16.0	15.0	6.7

3.2. Power Density and Material of Magnetic Core

At present, the energy harvesting devices developed at home and abroad are usually made of silicon steel, microcrystal alloy and permalloy as alternative materials for magnetic core [16-17]. Under the condition of no cutting, silicon steel has highly saturated magnetic induction intensity, the microcrystal alloy has high magnetic permeability, and the magnetic permeability of permalloy is intermediate between the two. Permalloy has the lowest saturated magnetic induction intensity.

From the analysis of air gap, it can be known that the magnetic core cutting will decrease the power output performance. To compare the power output characteristics of the three different magnetic cores before cutting, 20 samples are used for each type of the annular cores (no cutting), which are made by the three materials with internal diameter of 55 mm, external diameter of 85 mm, width of 20 mm and turns of 200. Then the circuit is shown as Fig. 3. The maximum output power of each magnetic core under 10 A primary current is observed. Whether the voltage waveform has distorted when the maximum power is reached is observed. If the distortion occurs, it means that the working point of the magnetic core has entered into the saturation region. The above magnetic core samples are cut by linear cutting. The value of load resistance is changed to measure the power output curve of magnetic core under 10 A primary current. The maximum output power is obtained. Fig. 9 shows the typical output curve after cutting.

Obviously, the power output of silicon steel magnetic core after cutting is significantly higher than that of the other two materials. The average values and variances of maximum output power P_{max} before cutting and those of maximum output power P'_{max} of the samples made by the three materials after cutting are calculated along with P'_{max} / P_{max}. The result is shown in Table 3.

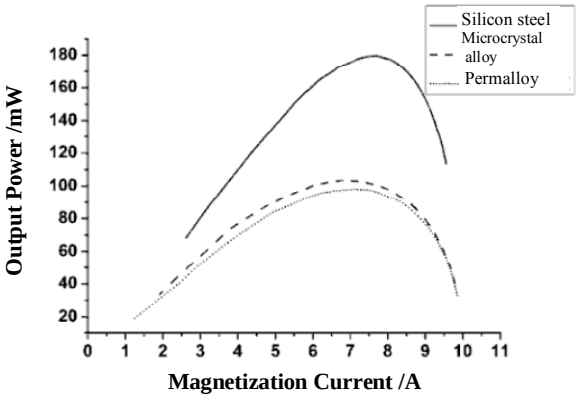

Fig. 9. Typical power output curves of magnetic cores in 3 materials.

From the standard deviations, it can be seen that the degree of concentration of the samples is relatively ideal. The output characteristics of the 20 magnetic cores of each material are consistent. Before cutting, the maximum output power of microcrystal alloy magnetic core under 10 A primary current is basically the same as that of silicon steel. However, the maximum power point of microcrystal alloy occurs in the saturation region, while the latter is in the linear area. Suppose that the equivalent air gap lengths caused by linear cutting of silicon steel and microcrystal alloy are equal. Then the magnetic permeability of microcrystal alloy in linear region is significantly higher than that of silicon steel after cutting. Further, the maximum output power of microcrystal alloy magnetic core should be significantly higher than that of silicon steel after cutting. However, the measured result is just the other way around. The average value of P'_{max} of microcrystal alloy magnetic core is only 57.5 % of that of P'_{max} of silicon steel after cutting. The P'_{max} / P_{max} of microcrystal alloy magnetic core is only 17.1%. All of these lead to the conclusion that the equivalent air gap length of microcrystal alloy magnetic core caused by linear cutting is certainly larger than that of silicon steel. Using formula (12), it can be estimated that the equivalent air gap length caused by cutting silicon steel is about 0.02 mm, while that of microcrystal alloy is at least 0.05 mm. By observing the sample section after cutting, it can be seen that the sections of silicon steel and permalloy samples are relatively smooth and clean, while the section of microcrystal alloy has an obvious rough surface. Mechanical polishing is performed for the microcrystal alloy magnetic core sample. Due to its large brittleness, a large amount of fragments is produced during polishing. By measuring the maximum output power of these magnetic core samples under 10 A primary current after polishing, the average value is 106.3 mW, and the standard deviation is 8.2 mW. It can be concluded that the mechanical polishing leads to no obvious improvement in the output characteristics of microcrystal alloy magnetic core.

Because the inductive energy harvesting magnetic core is assembled to the line, the magnetic core cannot be installed before cutting. The power density of permalloy magnetic core is the lowest after cutting, so it is not an alternative material for high power density magnetic core. Although the microcrystal alloy magnetic core without cutting has high magnetic permeability, due to its large brittleness and poor ductility [18], its performance will decline seriously after cutting. Besides, there will be phases transforming from amorphous state to crystalline state [19] at the kerf of microcrystal alloy when cutting. This will cause its magnetic performance to decline. Under the current cutting technology and polishing process, silicon steel is preferred as the magnetic core material in inductive energy harvesting device to get the maximum power density.

Degree has limit on magnetic core width. Besides, when the average magnetic path length is larger than one hour, the magnetic core will be easily saturated. Therefore, under permissible conditions, the internal and external diameter should be decreased and the magnetic core width be increased to obtain the maximum power density when designing the energy harvesting magnetic cores.

Table 3. Maximum output power of magnetic cores made of 3 materials before and after cutting.

Material	**Before cutting** P_{max}			**After cutting** P'_{max}			$\frac{P'_{max}}{P_{max}}$ **/%**
	Average value /mW	**Standard deviation /mW**	**Saturated or not**	**Average value /mW**	**Standard deviation /mW**	**Saturated or not**	
Silicon steel	603.2	16.77	No	179.8	6.87	No	29.8
Microcrystal alloy	605.1	13.58	Yes	103.4	7.94	No	17.1
Permalloy	352.1	9.45	Yes	98.0	7.23	No	27.4

4. Conclusions

This article establishes the power output model of energy harvesting magnetic core. Through theoretical analysis and experiment, the relationships of power density to air gap, the dimension and material of the magnetic core are verified. The conclusions are as follows:

1. The power output characteristics of energy harvesting coil can be described precisely using its load model.

2. Air gap has great effects on the output power of energy harvesting coil. Decreasing the air gap can improve its unit power density.

3. The performance of energy harvesting coils made by silicon steel is improved to a larger extent than that of microcrystal and permalloy in sequence.

Acknowledgements

This research was funded by a grant (No. 51307109) from the National Natural Science Foundation of China and a grant (No. S2013GR0102) from the International S&T Cooperation Projects of China.

References

[1]. N. M. Roscoe, M. D. Judd. J. Fitch, Development of magnetic induction energy harvesting for condition monitoring, in *Proceedings of the 44th International IEEE Universities Power Engineering Conference (UPEC)*, 2009, pp. 1-5.

[2]. J. Ahola T. Ahonen, V. Sarkimaki, et al., Design considerations for current transformer based energy harvesting for electronics attached to electric motor, , in *Proceedings of IEEE International Symposium on Power Electronics, Electrical Drives, Automation and Motion (SPEEDAM'08)*, 2008, pp. 901-905.

[3]. L. Xian-Zhi, D. Lin, C. Wei-Gen, et al., A novel scheme of draw-out power supply utilized in-transmission line state monitoring, *Automation of Electric Power Systems*, Vol. 32, Issue 1, 2008, pp.76-80.

[4]. W. Jintao, S. Gehao, Z. Yi, Design and Development of Power Supply for Transmission Line Online Monitor Device, *Electric Engineering*, Issue 2, 2009, pp. 33-35.

[5]. W. Zan, Z. Fei, W. Wei, et al., Development of Power Supply in High Voltage Side of Transmission Lines, *Advances of Power System and Hydroelectric Engineering*, Issue 6, 2010, pp. 23-27.

[6]. T. Xu-hui, W. Bao-juan, Z. Jing-chao, etc., Design of Power Supply for Optical Current Transformer in High Voltage Side, *High-voltage Electrical Appliances*, Vol. 45, Issue 5, 2009, pp. 123-125.

[7]. R. Xiaodong, C. Shuyong, J. Tao, Design of a High Side Energy Extracting Device for Active Electronic Current Transformer, *Power System Technology*, Vol. 32, Issue 18, 2008, pp. 67-71.

[8]. G. Yingxia, Research of the High Voltage Circuit and Power Supply for Electronic Current Transformer, *Yanshan University*, 2006.

[9]. P. Tao, X. Lei, Y. Chun, et al., Development of HV Side Power Supply for Electronic Current Transformer, *Transformer*, Vol. 47, Issue 5, 2010, pp. 5-7.

[10]. Q. Dong, A Kind of Power Supply of Optic-electric Current Transformer for Accommodating Wide Bus Dynamic Current, in *Proceedings of the CSEE*, Vol. 26, Issue 19, 2006, pp. 160-164.

[11]. L. Yadong, S. Gehao, W. Kui etc., Design of Current Transformer Energy Harvesting Power Supply Based on Phase Angle Control Method, *Automation of Electric Power Systems*, Vol. 35, Issue 19, 2011, pp. 72-76.

[12]. L. Yadong, Studies on Distributed Fault Location Theory and the Key Technologies for Transmission Line, *Shanghai Jiaotong University*, 2012.

[13]. Z. Shunrong, Electro mechanics, 2nd edition. *Beijing: Science Press*, 2007.

[14]. L. Ya-dong, S. Ge-hao, W. You-jia, etc., Current Transformer Draw-out Power Supply Design Based on Power-controlled Method, *Automation of Electric Power Systems*, Vol. 34, Issue 3, 2010, pp. 70-74.

[15]. W. M. Flanagan, Handbook of Transformer Design and Applications, 2nd edition, New York, *McGraw-Hill*, 1993.

[16]. L. Jie, L. Gang, Z. Ming, Impact Analysis for the Air-gap Width of Draw-out Power Supply Coil, *High Voltage Apparatus,* Vol. 48, Issue 12, 2012, pp. 75-79.

[17]. G. Lin-Yun, Y. Xiang-Gen, Y. Xin-Rong, et al., Research of Improving Power Efficiency for Intelligent Device Self-power Supply Utilized in Power Distribution Network, in *Proceedings of the CSEE*, Vol. 29, Issue 1, 2009, pp. 217-221.

[18]. Z. Guoxiang, A New Fe-based Amorphous Alloy with Excellent Soft Magnetic Properties, *Metallic Functional Materials*, Vol. 10, Issue 2, 2003, pp. 13-18.

[19]. Liu Ji-Lei, Zhu Zheng-Hou, Yin Lei, at al., Effect of wire saw technique on the soft magnetic properties of Fe78Si9B13 amorphous alloy under line frequency, *Journal of Nanchang University (Natural Science)*, Vol. 36, Issue 4, 2012, pp. 351-354.